# Chapter 6
# Thin Plates

The chapter is devoted to buckling, postbuckling behaviour and dynamic buckling of thin plates made of metals or composites modelled as orthotropic materials. The considered plates are simply supported on loaded edges and different boundary condition on longitudinal edges. They are subjected to uniform compression.

All calculations were performed assuming elastic homogenous material properties. Isotropic and orthotropic materials were considered (Table 6.1).

All materials mentioned in Table 6.1 are isotropic, hence, the Kirchhoff's modulus can be calculated according to following well known equation:

$$G = \frac{E}{2(1-v)}. \tag{6.1}$$

The fibre composite material was modelled as orthotropic but for components (resin and fibre), isotropic material properties (Table 6.1) were assumed. Necessary equations for material properties homogenization based on the theory of mixture [2, 3] are as follows:

$$\begin{aligned} E_x &= E_m(1-f) + E_f f, \\ E_y &= E_m \frac{E_m(1-\sqrt{f}) + E_f\sqrt{f}}{E_m[1-\sqrt{f}(1-\sqrt{f})] + E_f\sqrt{f}(1-\sqrt{f})}, \\ v_{yx} &= v_m\left(1-\sqrt{f}\right) + v_f\sqrt{f}, \\ G &= G_m \frac{G_m\sqrt{f}(1-\sqrt{f}) + G_f[1-\sqrt{f}(1-\sqrt{f})]}{G_m\sqrt{f} + G_f(1-\sqrt{f})}, \end{aligned} \tag{6.2}$$

where $E_m$ and $E_f$ are the Young's modulus of elasticity for matrix and fibre, respectively, $G_m$ and $G_f$ are the shear modulus for matrix (subscript $m$) and fibre (subscript $f$), $v_m$ and $v_f$ are Poisson's ratios for matrix and fibre, and $f = V_f/(V_m + V_f)$ is the fibre volume fraction.

It should be noticed that taking into account (6.2) and the volume fibre fraction $f$ from the range 0.2 to 0.7, the coefficient of orthotropy defined as $E_x/E_y$ varies from 2.9 to 3.6. Moreover, in real, industrially produced structures, the

T. Kubiak, *Static and Dynamic Buckling of Thin-Walled Plate Structures*,
DOI: 10.1007/978-3-319-00654-3_6,

**Table 6.1** Assumed material properties

| Material type | $E$ (GPa) | $v$ | $\rho$ (kg/m$^3$) |
|---|---|---|---|
| Steel | 200 | 0.3 | 7,850 |
| Aluminium | 70 | 0.33 | 2,950 |
| Epoxy resin | 3.5 | 0.33 | 1,249 |
| Glass fibre | 71 | 0.22 | 2,450 |

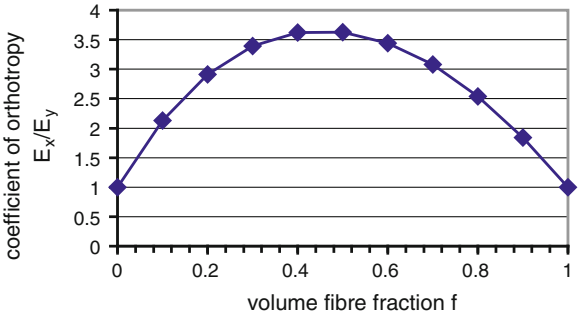


**Fig. 6.1** Volume fibre fraction influence on coefficients of orthotropy for fibre glass epoxy resin

above-mentioned volume fibre fraction $f$ ranges from 0.4 to 0.6, so in our case the coefficient of orthotropy varies from 3.4 to 3.6. Figure 6.1 shows a relation between the volume fibre fraction and the coefficient of orthotropy for glass fibre in epoxy resin with the material data presented in Table 8.1.

Rectangular thin plates simply supported on loaded edges with different boundary conditions along the unloaded edges were considered (Fig. 6.2). On the longitudinal edges, five different boundary condition cases were taken into account. The following notations are used in Fig. 6.2: s—simply supported edge, c—clamped edge, e—free edge.

Plates with constant and variable material properties were considered. Composite plates with the widthwise variable volume fibre fraction were modelled by dividing the plate into strips (Fig. 6.3) with constant material properties assigned to the assumed volume fibre fraction $f$. Its value was determined on the basis of the arbitrary adopted sine function:

$$f = f_{av} + A \cdot \cos\left(\frac{2\pi y}{b}\right), \tag{6.3}$$

where: $f_{av} = 0.5$—arbitrary assumed average value of the fibre volume fraction; $A = < -0.4;\ 0.4 >$—amplitude of sine describing the change of material properties along the plate width. The range of the amplitude is assumed in such a way that the volume fibre fraction $f$ varies from 0.1 to 0.9 or from about 10 % to 90 % of reinforcing fibres in the composite structure. However, the proposed method allows one to analyse any function describing a widthwise variation of material properties, not necessarily that one defined by changes in the volume fibre fraction content $f$ [6, 7].

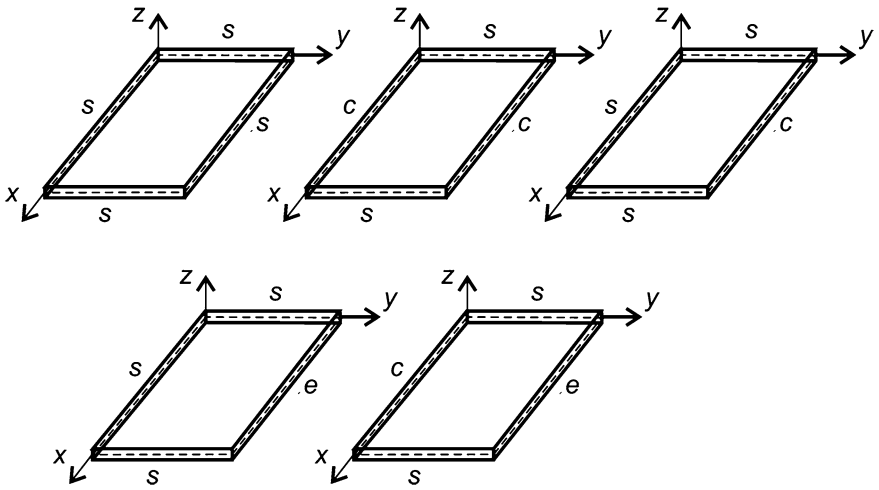


**Fig. 6.2** Analysed plates with different boundary conditions

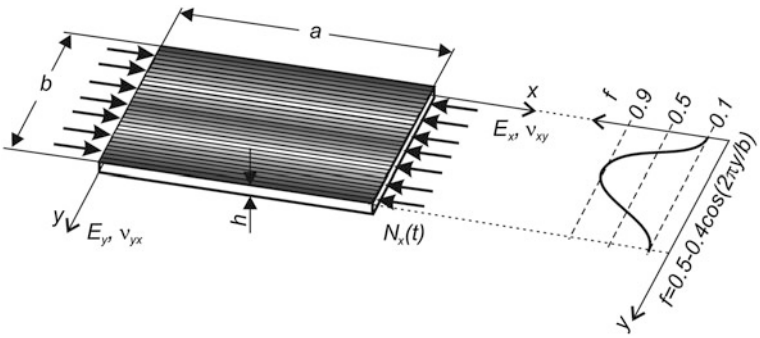


**Fig. 6.3** Model of the plate with widthwise sinusoidally variable material properties (volume fibre fraction)

The results presented further were obtained using the analytical-numerical method (MAN) and the finite element method (FEM) software.

In the dynamic buckling analysis, load is defined as a dynamic load factor, i.e., an amplitude of the pulse load divided by the static buckling load. Therefore, the static buckling load and the corresponding buckling mode should be determined. The buckling mode is used to map an initial imperfection on the plate midplane. The time of pulse duration is assumed as corresponding to a period of natural vibrations. It means that the eigenvalue modal analysis and the eigenbuckling analysis should be performed in the first stage.

The natural frequencies and the buckling load for composite and steel square plates ($a/b = 1$) with the thickness ratio $b/h = 100$ for different boundary condition cases are presented in Table 6.2.

**Table 6.2** Buckling load and natural frequencies for the plates under analysis

| Material | Boundary conditions | Buckling load $P_{cr}$ (kN) | | Natural frequencies $\omega$ (rad/s) | |
|---|---|---|---|---|---|
| | | MAN | FEM | MAN | FEM |
| Steel | ss | 7.23 | 7.24 | 3016 | 3010 |
| | cc | 15.55 ($m = 1$) | 15.66 | 4423 ($m = 1$) | 4423 |
| | | 13.90 ($m = 2$) | 14.02 | 8363 ($m = 2$) | 8344 |
| | se | 2.53 | 2.54 | 1784 | 1784 |
| | ce | 2.99 | 2.99 | 1935 | 1935 |
| | sc | 10.38 | 10.41 | 3613 | 3607 |
| Glass fibre epoxy resin composite with $f = 0.2$ | ss | 0.28 | 0.28 | 1351 | 1351 |
| | cc | 0.50 | 0.51 | 1822 | 1822 |
| | se | 0.16 | 0.16 | 1030 | 1030 |
| | ce | 0.17 | 0.17 | 1062 | 1062 |
| | sc | 0.36 | 0.36 | 1546 | 1546 |
| Glass fibre epoxy resin composite with $f = 0.5$ | ss | 0.54 | 0.54 | 1703 | 1709 |
| | cc | 0.93 | 0.95 | 2231 | 2237 |
| | se | 0.34 | 0.35 | 1351 | 1351 |
| | ce | 0.36 | 0.37 | 1389 | 1389 |
| | sc | 0.69 | 0.70 | 1916 | 1923 |
| Glass fibre epoxy resin composite with $f = 0.7$ | ss | 0.81 | 0.82 | 1954 | 1960 |
| | cc | 1.44 | 1.46 | 2608 | 2620 |
| | se | 0.48 | 0.48 | 1502 | 1502 |
| | ce | 0.51 | 0.51 | 1558 | 1558 |
| | sc | 1.05 | 1.06 | 2224 | 2231 |

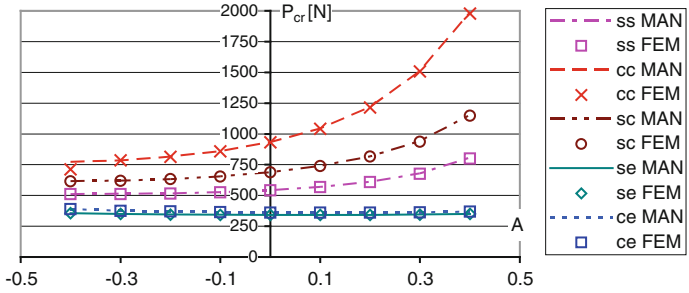


**Fig. 6.4** Static buckling load $P_{cr}$ as a function of the amplitude $A$ describing the distribution of the volume fibre fraction

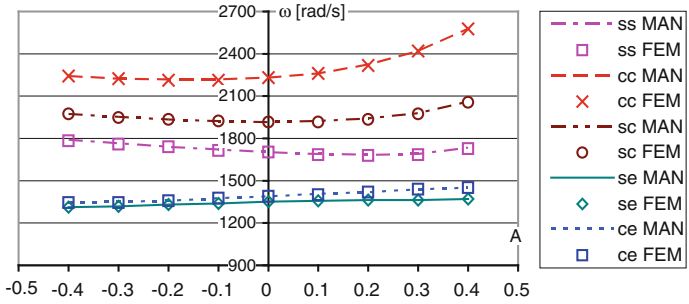


**Fig. 6.5** Natural frequencies as a function of the amplitude $A$ describing the distribution of the volume fibre fraction

The natural frequencies and the buckling load for the square composite plate ($a/b = 1$, $b/h = 100$) with the widthwise variable volume fibre fraction (6.3) for different amplitudes A (describing the volume fibre fraction distribution) are presented in Figs. 6.4 and 6.5, respectively. For all boundary condition cases, both the employed methods of calculations give similar results, which confirms the correctness of the calculations.

As can be seen in Figs. 6.4 and 6.5, the buckling loads as well as the natural frequencies grow with an increasing value of the amplitude $A$ describing the volume fibre fraction in the plate widthwise direction. This means that plates with stiffer longitudinal strips near the plate edges are stiffer as a whole (a higher buckling load and higher natural frequencies) than plates with a stiffer central longitudinal strip.

## 6.1 Postbuckling Behaviour

The postbuckling behaviour analysis allows one to describe the behaviour of the plate subjected to a load higher than the buckling load. Postbuckling equilibrium paths for a steel square plate with different boundary conditions on longitudinal edges subjected to uniform compression (uniform shortening—see Fig. 6.11) are presented in Fig. 6.6. Equilibrium paths for an ideal flat plate are presented in Fig. 6.6a and for a plate with geometrical imperfections with the amplitude $\xi^* = 0.01$—in Fig. 6.6b, correspondingly.

For an ideal plate structure, the critical load can be determined from the eigenvalue analysis but for structures with imperfections, the buckling load may be determined on the basis of the pre- and post- buckling behaviour. Two well-known methods for identification of the critical load were employed. They are usually applied to the results of experimental investigations. The inflection point method (P-w), which is very similar to the "top of the knee" method and the alternative ($P\text{-}w^2$) method were used.

An influence of initial imperfection amplitudes $\xi^*$ on postbuckling equilibrium paths for epoxy glass composite (fibre volume factor $f = 0.5$) square plates simply supported on all edges was investigated. The obtained results in the form of postbuckling curves presented as the nondimensional load $P/P_{cr}$ versus nondimensional displacement $\xi = w/h$ (where $h$ is the plate thickness) are shown in Fig. 6.7. Using the inflection point and alternative methods, the buckling load $P^*_{cr}/P_{cr}$ (where $P^*_{cr}$—buckling compressive force for an imperfect plate and $P_{cr}$—bifurcation load) for a plate with geometrical imperfections was found and is presented in Table 6.3.

The results shown in Table 6.3 allow one to conclude that lower values of $P^*_{cr}$ were obtained using the $P\text{-}w^2$ method and the differences between the results of both the methods grow with an increase in the imperfection amplitude value. It can also be noted that the higher initial imperfection amplitude, the lower critical buckling load.

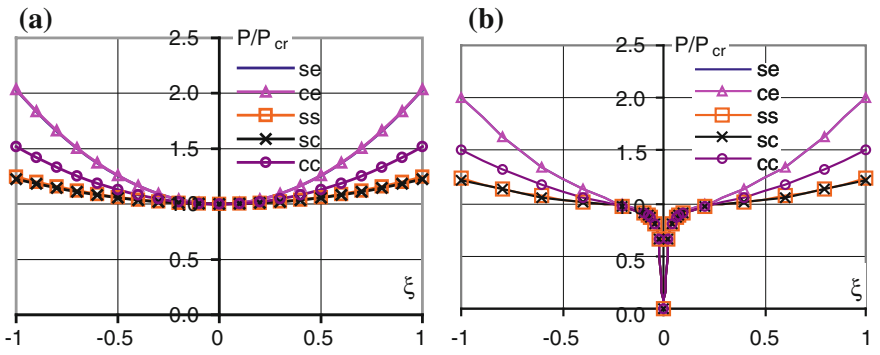


**Fig. 6.6** Postbuckling equilibrium paths for square ideal plates (**a**) and plates with imperfections (**b**) with different boundary conditions on non-loaded edges

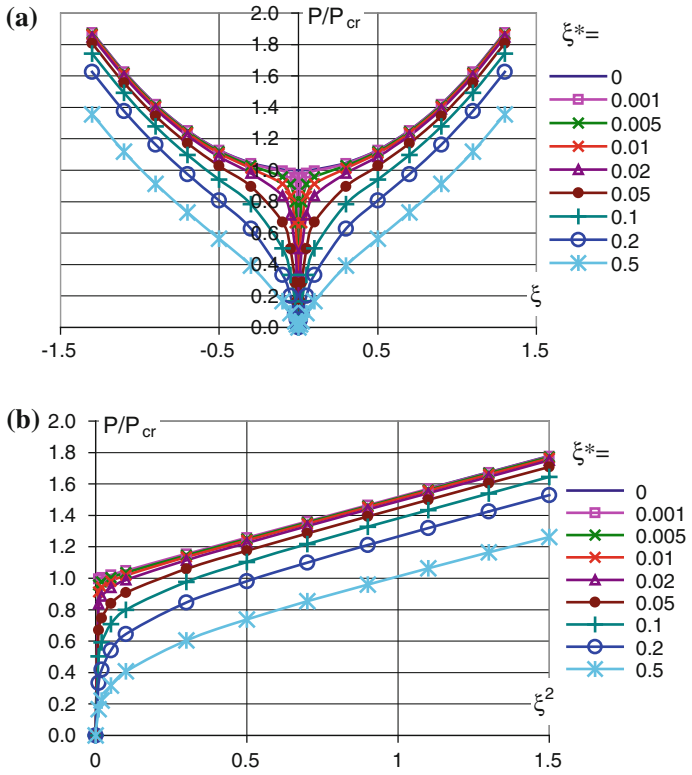


**Fig. 6.7** Dimensionless load $P/P_{cr}$ versus dimensionless deflection (**a**) or square of dimensionless deflection (**b**)

**Table 6.3** $P^*_{cr}/P_{cr}$ for different amplitudes of initial imperfections

| Determination method: initial imperfection amplitude $\xi^*$ | P-w $P^*_{cr}/P_{cr}$ | P-w$^2$ $P^*_{cr}/P_{cr}$ |
|---|---|---|
| 0.001 | 0.999 | 0.999 |
| 0.005 | 0.998 | 0.994 |
| 0.01 | 0.995 | 0.986 |
| 0.02 | 0.990 | 0.968 |
| 0.05 | 0.968 | 0.925 |
| 0.1 | 0.925 | 0.863 |
| 0.2 | 0.834 | 0.751 |
| 0.5 | 0.589 | 0.494 |

An influence of the initial imperfection amplitude on the critical buckling load and the postbuckling behaviour was checked for the rest of the assumed boundary conditions (Fig. 6.2). Some exemplary postbuckling equilibrium paths obtained with MAN for rectangular composite (volume fibre fraction $f = 0.5$) plates are

presented in Figs. 6.8 and 6.9. The results for an ideal plate are presented in Fig. 6.8 and for a plate with the initial imperfection amplitude $\xi^* = 0.1$—in Fig. 6.9. The relations between the critical load for the plate with imperfections and the ideal flat plate for different initial imperfection amplitudes $\xi^*$ are presented in Tables 6.4 and 6.5, correspondingly.

Comparing the results presented in Tables 6.4 and 6.5, a similar conclusion to those based on the results in Table 6.3 can be drawn, i.e., differences between the results of both the methods grow with an increase in the imperfection amplitude value and the higher initial imperfection amplitude, the lower critical buckling load.

Let us compare postbuckling equilibrium paths for a plate made of steel and composite with all simply supported edges (the case denoted by "ss" in Fig. 6.2) and with one free edge (the case denoted by "se" in Fig. 6.2). A comparison of the results is presented in Fig. 6.10.

The results presented in Fig. 6.10 show that the plate made of a composite material is stiffer due to its orthotropic character than the plate made of steel. It should be emphasized that the results presented are nondimensional so for a dimensional value of the buckling load, the steel plate has a higher value than the

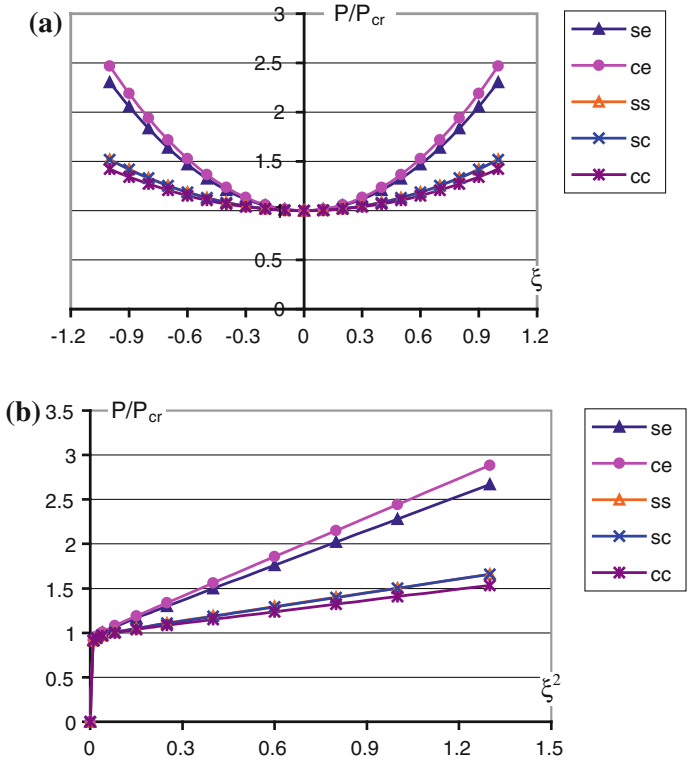


**Fig. 6.8** Postbuckling equilibrium paths for ideal flat composite plates obtained from P-w (**a**) and P-$w^2$ (**b**) methods

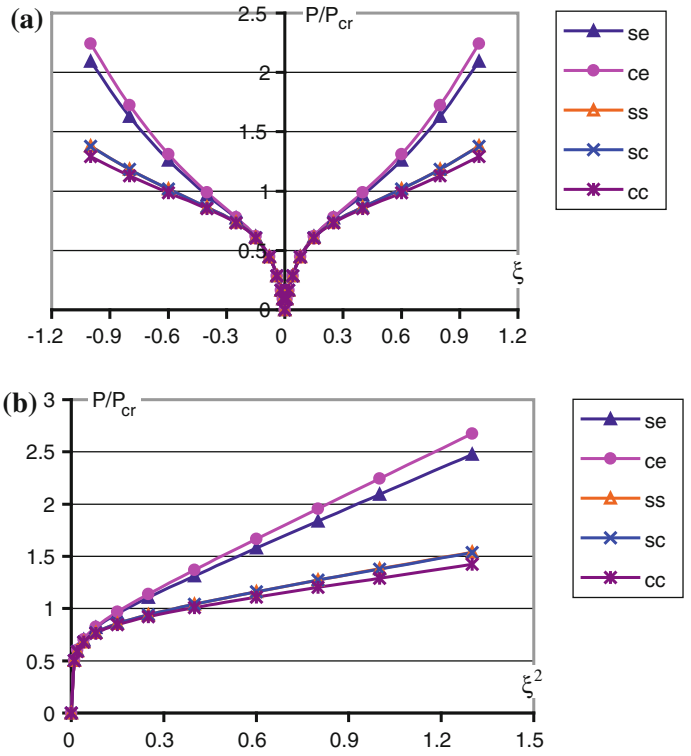


**Fig. 6.9** Postbuckling equilibrium paths for plates with imperfections $\xi^* = 0.1$ obtained from P-w (**a**) and P-$w^2$ (**b**) methods

**Table 6.4** $P^*_{cr}/P_{cr}$ determined with the "top of the knee" method—P-w method

| $\xi^*$ = boundary conditions | 0.01 | 0.1 | 0.5 |
|---|---|---|---|
| se | 0.99 | 0.87 | 0.42 |
| ce | 0.99 | 0.86 | 0.39 |
| ss | 1 | 0.93 | 0.59 |
| sc | 1 | 0.93 | 0.59 |
| cc | 1 | 0.93 | 0.62 |

**Table 6.5** $P^*_{cr}/P_{cr}$ determined with the alternative method—P-$w^2$ method

| $\xi^*$ = boundary conditions | 0.01 | 0.1 | 0.5 |
|---|---|---|---|
| se | 0.97 | 0.77 | 0.38 |
| ce | 0.97 | 0.76 | 0.37 |
| ss | 0.97 | 0.79 | 0.43 |
| sc | 0.97 | 0.79 | 0.43 |
| cc | 0.97 | 0.79 | 0.44 |

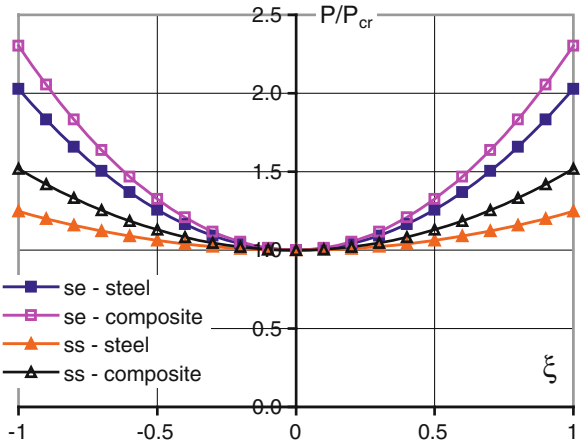


**Fig. 6.10** Postbuckling equilibrium paths for steel and composite plates

composite one due to differences in their Young's modulus. A comparison of the boundary conditions (compare the curve denoted as "ss" and "se" in Fig. 6.10 for the chosen material), which do not depend on material properties (relations for the steel plate and the composite plate are the same), is very interesting—in the case when one longitudinal edge is free, the plates are stiffer than in the case when all edges are simply supported. The stiffness relation describe above seems to be unrealistic, but as will be shown below, the above-mentioned relation depends on the assumed boundary conditions at the loaded edge. In the model under investigation, the boundary conditions on loaded edges were assumed in such a way that the edges were straight and remained parallel during loading (Fig. 6.11).

A comparison between compressed simply supported plates with one longitudinal edge free for two different assumptions can be found in [5] and is presented in Fig. 6.12. The curve denoted by '1' was obtained on the assumption that the loaded edges were straight and remained parallel during loading. The curve denoted as '2' was obtained on the assumption that the loaded edges were straight and could rotate about normal to the middle surface plane. Comparing the postbuckling equilibrium paths denoted as 1 and 2 in Fig. 6.11, an influence of the assumed boundary conditions is very well visible. Additionally, in Fig. 6.11, a postbuckling path for the plate with all simply supported edges is presented and denoted as '3'.

## 6.2 Dynamic Buckling

Having determined the natural vibration frequency, the static buckling load with the corresponding buckling mode and postbuckling equilibrium paths for plates with initial geometrical imperfections, a dynamic response analysis can be performed for

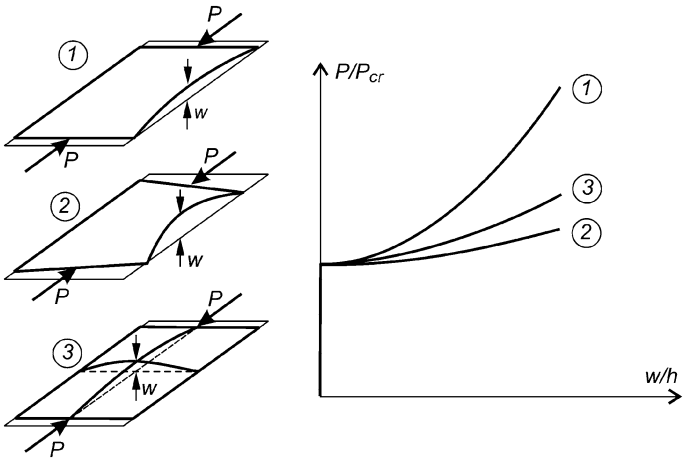


**Fig. 6.11** Postbuckling equilibrium paths for plates with different assumptions on loaded edges

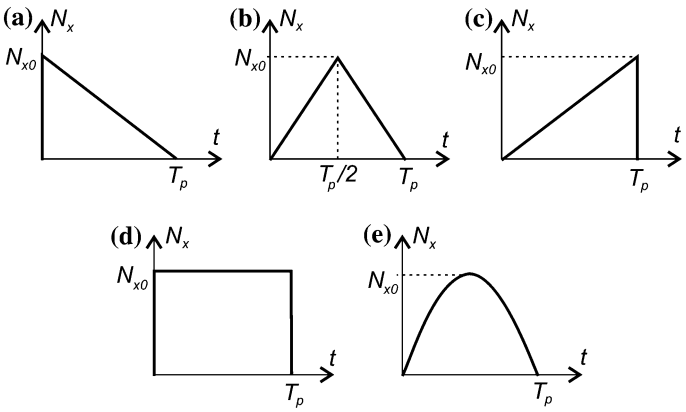


**Fig. 6.12** Pulse load shapes denoted as: **a** T1, **b** T2, **c** T3, **d** P, **e** S

plates subjected to the pulse load (Fig. 6.12) of a rectangular (P), three triangular type (descending T1, equilateral T2 and T3 growing) and sinusoidal (S) shape.

In order to verify the analytical-numerical method, the finite element analysis was performed and the obtained results were compared to the results presented by Petry and Fahlbusch [12]. Figure 6.13 shows a dimensionless maximum deflection as a function of the dynamic load factor *DLF* for the aluminium square plate ($a/b = 1$ and $b/h = 200$) simply supported on all edges and subjected to compression with a sinusoidally shaped pulse load. The duration of the pulse corresponds to the period of natural vibrations for the plate under consideration. The amplitude of initial imperfections was assumed to be equal to 5/100 of the plate thickness.

The analytical-numerical method presented in Chap. 3 gives a slightly higher deflection value than the results presented in the literature [12] and obtained from the finite element method. The higher differences of the *DLF* value increase from about 2 % for the $DLF = 1.2$ up to 14 % for the $DLF = 4$. The discrepancies for the growing pulse load amplitude may be due to a more accurate model adopted by Petry and Fahlbusch [12], who took a relatively larger number of terms in the series function describing the plate deflection in the solution. It should be noted that the proposed approach allows one to determine well enough the critical value of the dynamic load factor $DLF_{cr}$ according to the Volmir or Budiansky-Hutchinson criterion (see Table 6.6).

Other examples which confirm the correctness of the applied methods of computations can be found in the monograph edited by Kowal-Michalska [4]. Therefore, in the following part of the study, the results obtained only with the two employed methods of calculations, i.e., the finite element method (FEM) and the analytical-numerical method (MAN), will be compared.

Dynamic buckling of thin plates, as shown in the literature overview (Sect. 1.3.2), is the subject of many papers and has appeared in the literature for more than 50 years. The author of this monograph in his previous works [4, 8–10] analysed different shapes of pulse loading, an influence of material properties and boundary conditions on unloaded edges of plates. Below, a summary of the results contained in those works is presented. The results are compared to the results obtained with methods known from experimental investigations, i.e., the inflection point and alternative method (see Sect. 5.8).

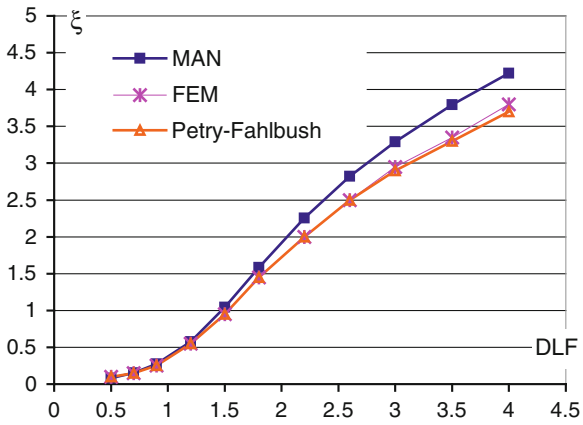


**Fig. 6.13** Curves $\xi$ (DLF) for the aluminium plate—a comparison of the results

**Table 6.6** Critical value of *DLF* obtained with different methods

| Criterion/method | Budiansky-Hutchinson | Volmir $\xi = 1$ |
|---|---|---|
| MAN | 1.5–1.8 | 1.48 |
| FEM | 1.5–1.8 | 1.53 |
| Petry-Fahlbusch | 1.5–1.8 | 1.52 |

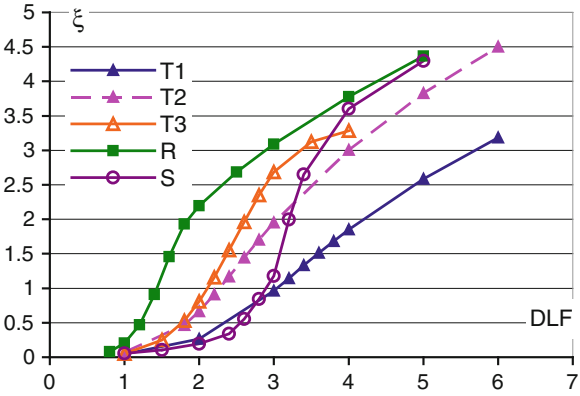


**Fig. 6.14** Dynamic response curves for the simply supported plate—a comparison of the pulse load shape

A different shape of the pulse loading influence on dynamic responses of the plate is shown in Figs. 6.14 and 6.15 and in Table 6.7. Figure 6.14 presents some exemplary results obtained from the analytical-numerical method for the plate made of a composite with the volume fibre fraction equal to $f = 0.5$ and clamped on longitudinal edges ('cc'). In Fig. 6.15, a comparison of the results obtained with the analytical-numerical method (MAN) and the finite element method (*FEM*) for triangularly (*T1*) and rectangularly (*R*) shaped pulses is presented. The curves in Fig. 6.15 present the results for the simply supported plate made of an epoxy-glass composite with the volume fibre fraction equal to $f = 0.5$. The results obtained from both the methods are consistent.

The Budiansky-Hutchinson and Volmir criteria were compared for a square plate with the fibre volume fraction $f = 0.8$, for all the boundary conditions and impulses under analysis. The obtained critical value of dynamic load factors $DLF_{\mathrm{cr}}$ are presented in Table 6.7.

The dimensionless critical value of the dynamic load factor $DLF_{\mathrm{cr}}$ determined according to the Budiansky-Hutchinson criterion, the Volmir criterion, author's modification of the Kleiber-Kotula-Saran criterion and the methods known from

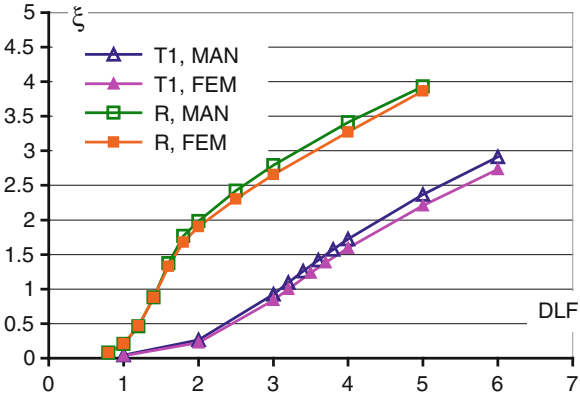


**Fig. 6.15** Dynamic response curves for the simply supported plate—a comparison of calculation methods

**Table 6.7** *DLF*s for the fibre volume fraction equal to f = 0.8

| | T1 | | T2 | | T3 | | R | | S | |
|---|---|---|---|---|---|---|---|---|---|---|
| | Budiansky-Hutchinson | Volmir | Budiansky-Hutchinson | Volmir | Budiansky-Hutchinson | Volmir | Budiansky-Hutchinson | Volmir | Budiansky-Hutchinson | Volmir |
| ss | 3.1–3.3 | 3.1 | 2.4–2.6 | 2.3 | 2.4–2.6 | 2.1 | 1.4–1.6 | 1.4 | 3.0–3.2 | 2.9 |
| cc | 3.2–3.4 | 3.0 | 2.4–2.6 | 2.2 | 2.5–2.7 | 2.1 | 1.4–1.6 | 1.4 | 3.0–3.2 | 2.9 |
| cs | 3.2–3.4 | 3.1 | 2.4–2.6 | 2.3 | 2.4–2.6 | 2.1 | 1.4–1.6 | 1.4 | 3.0–3.2 | 2.9 |
| se | 2.8–3.0 | 3.6 | 2.0–2.2 | 2.6 | 2.0–2.2 | 2.2 | 1.2–1.4 | 1.6 | 3.0–3.2 | 3.0 |
| ce | 2.8–3.0 | 3.6 | 2.0–2.2 | 2.6 | 2.0–2.2 | 2.2 | 1.2–1.4 | 1.7 | 3.0–3.2 | 3.1 |

experimental studies (i.e., inflection point and alternative methods) for steel and composite plates subjected to a rectangularly shaped pulse load (with a duration corresponding to the period of natural vibrations) are summarized in Tables 6.8 and 6.9. The results were obtained with the analytical-numerical method on the assumption that the amplitude of initial geometrical imperfections was equal to $\xi^* = 0.01$.

The dimensionless critical dynamic load factor values presented in Tables 6.8 and 6.9 confirm a compliance of the new criterion and the new approach with the well-known Budiansky-Hutchinson and Volmir criteria. However, the alternative method used to determine the critical dynamic buckling amplitude yields the results about twice lower than the other applied methods. This means that the alternative method should rather not be used to determine the critical value of *DLF*, so in the further part of the presentation of the results, it will not be used. In the case of plates with boundary conditions denoted as "se" and "ce", the results

**Table 6.8** $DLF_{cr}$ comparison for steel plates

| Boundary condition | Mode $m$ | Critical value of the dynamic load factor $DLF_{cr}$ | | | | |
|---|---|---|---|---|---|---|
| | | Budiansky-Hutchinson | Volmir $\xi = 1$ | Author's criterion $r_{max} = 1$ | P-w | P-w$^2$ |
| ss | 1 | 1.5–1.6 | 1.43 | 1.51 | 1.67 | 0.76 |
| cc | 2 | 1.4–1.5 | 1.51 | 1.38 | 1.50 | 0.69 |
| se | 1 | 1.5–1.6 | 1.55 | 1.35 | 1.22 | 0.59 |
| ce | 1 | 1.3–1.4 | 1.58 | 1.35 | 1.22 | 0.59 |
| sc | 1 | 1.4–1.8 | 1.46 | 1.58 | 1.70 | 0.76 |

**Table 6.9** $DLF_{cr}$ comparison for epoxy-glass composite plates

| Volume fibre fraction $f$ | Boundary condition | Mode $m$ | Critical value of the dynamic load factor $DLF_{cr}$ | | | | |
|---|---|---|---|---|---|---|---|
| | | | Budiansky-Hutchinson | Volmir $\xi = 1$ | Author's criterion $r_{max} = 1$ | P-w | P-w$^2$ |
| 0.2 | ss | 1 | 1.45–1.6 | 1.46 | 1.46 | 1.52 | 0.69 |
| | cc | 1 | 1.45–1.6 | 1.44 | 1.49 | 1.53 | 0.72 |
| | se | 1 | 1.3–1.45 | 1.65 | 1.31 | 1.15 | 0.55 |
| | ce | 1 | 1.3–1.45 | 1.68 | 1.30 | 1.10 | 0.52 |
| | sc | 1 | 1.6–1.75 | 1.45 | 1.46 | 1.52 | 0.70 |
| 0.5 | ss | 1 | 1.45–1.5 | 1.46 | 1.45 | 1.45 | 0.69 |
| | cc | 1 | 1.45–1.6 | 1.45 | 1.48 | 1.52 | 0.71 |
| | se | 1 | 1.3–1.45 | 1.64 | 1.31 | 1.14 | 0.54 |
| | ce | 1 | 1.3–1.45 | 1.71 | 1.30 | 1.10 | 0.52 |
| | sc | 1 | 1.3–1.45 | 1.46 | 1.44 | 1.45 | 0.69 |
| 0.7 | ss | 1 | 1.3–1.45 | 1.34 | 1.32 | 1.43 | 0.66 |
| | cc | 1 | 1.45–1.6 | 1.44 | 1.49 | 1.53 | 0.72 |
| | se | 1 | 1.3–1.45 | 1.61 | 1.31 | 1.15 | 0.55 |
| | ce | 1 | 1.3–1.45 | 1.70 | 1.30 | 1.10 | 0.52 |
| | sc | 1 | 1.45–1.6 | 1.46 | 1.46 | 1.46 | 0.70 |

obtained with author's criterion differ by about 10 % and by 15 % when the inflection point method is used. In other cases (excluding the alternative method), they are between the values of the criteria designated by Budiansky-Hutchinson and Volmir. The best agreement of the results was achieved for plates with supported edges (i.e., the boundary condition denoted as 'ss', 'sc', 'cc') between the following two pairs: author's criterion—the Volmir criterion and the Budiansky-Hutchinson criterion—the inflection point method.

In the literature [1, 13–15], the dynamic buckling occurs when the pulse duration is close to a period of fundamental vibrations or to half a period of fundamental vibrations [1] and the initial deflection is very small in relation to the thickness of the plate. Therefore, the simply supported composite plate made of an epoxy-glass composite with the volume fibre fraction $f = 0.5$ subjected to rectangular pulse load was taken as an example to analyse an influence of pulse duration and the assumed initial imperfection amplitude on the dynamic response. The results are shown in Figs. 6.16 and 6.17 and are summarized in Tables 6.10 and 6.11, respectively.

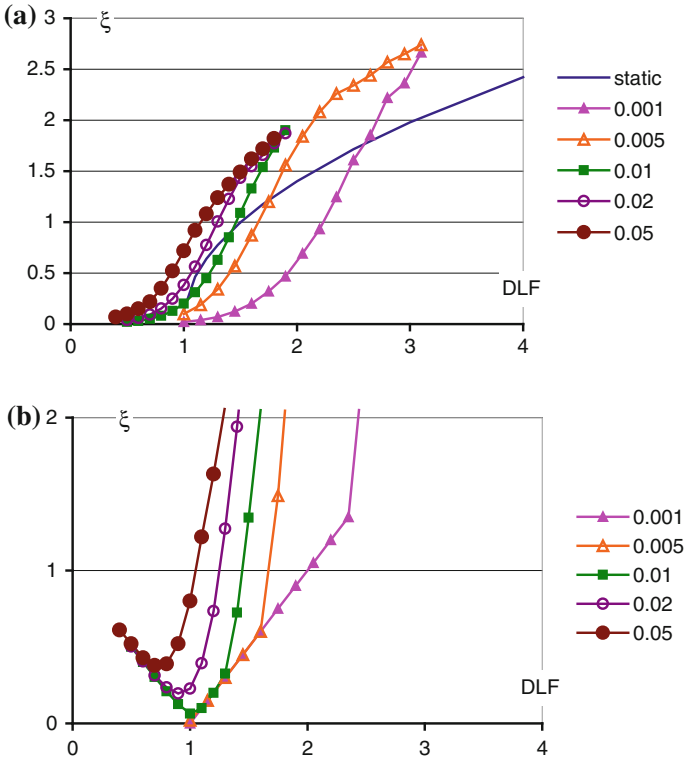


**Fig. 6.16** Influence of the initial imperfection amplitude on the course of the curves $\xi$ (*DLF*) and $r_{max}$ (*DLF*) for the simply supported composite plate

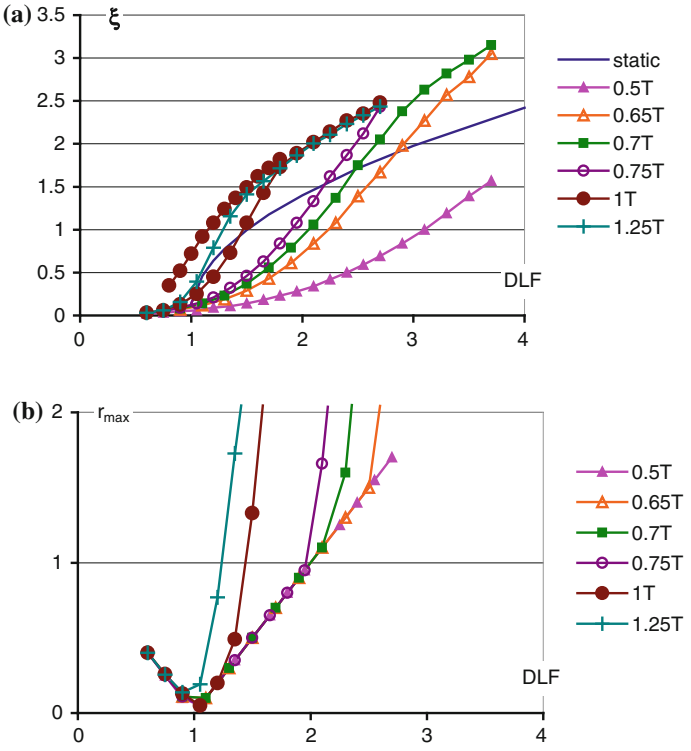


**Fig. 6.17** Influence of the pulse duration on the course of the curves $\xi$ (*DLF*) and $r_{\max}$ (*DLF*) for the simply supported composite ($f = 0.5$) plate

In Fig. 6.16, a postbuckling static equilibrium path for the ideal flat plate is also presented. The curves $\xi$ (*DLF*) for a large amplitude of initial imperfections do not cross the postbuckling equilibrium path, which would suggest that for such large initial imperfections, the critical dynamic load factor is equal or even less than the static buckling load. However, the results summarized in Table 6.10 show that this is not entirely true and a decrease in $DLF_{\mathrm{cr}}$ with an increase in the amplitude of initial imperfections is observed.

**Table 6.10** Influence of the amplitude of initial imperfections on $DLF_{\mathrm{cr}}$

| Amplitude of initial imperfections $\xi^*$ | Critical value of the dynamic load factor $DLF_{\mathrm{cr}}$ | | | |
|---|---|---|---|---|
| | Budiansky-Hutchinson | Volmir $\xi = 1$ | Author's criterion $r_{max} = 1$ | Inflection point method *P-w* |
| 0.001 | 2.35–2.5 | 2.23 | 2.00 | 2.40 |
| 0.005 | 1.75–1.9 | 1.66 | 1.67 | 1.68 |
| 0.01 | 1.45–1.5 | 1.46 | 1.45 | 1.52 |
| 0.02 | 1.2–1.3 | 1.30 | 1.25 | 1.31 |
| 0.05 | 1.0–1.1 | 1.15 | 1.05 | 1.14 |

Figure 6.17 shows the curves $\xi$ ($DLF$) for different pulse durations. Additionally, a postbuckling static equilibrium path for the ideal flat plate is depicted. The presented curves (excluding the postbuckling equilibrium path) were calculated with the assumed amplitude of initial imperfections $\xi^* = 0.01$. Similarly as in the case of the curves presented in Fig. 6.16a, only a few curves in Fig. 6.17a intersect the postbuckling equilibrium path—it takes place for the curves calculated with a pulse duration less than $1.25T$ (where $T$ is a period of the natural frequency of vibrations). Analysing the results presented in Table 6.11, one can see that an extension of the pulse duration leads to $DLF_{\mathrm{cr}} = 1$, i.e., to the same results as for the static buckling load.

As has been stated previously, on the basis of the results summarized in Tables 6.8 and 6.9, it can be said that the critical dynamic load factor $DLF_{\mathrm{cr}}$ resulting from the proposed criterion can be found between the results obtained with application of the Volmir criterion and the Budiansky-Hutchinson criterion. The inflection point method gives similar results as for the Budiansky-Hutchinson criterion. This fact is also confirmed by the majority of the results shown in Figs. 6.16 and 6.17 and Tables 6.10 and 6.11. An advantage of the inflection point method over the Budiansky-Hutchinson criterion is a possibility to determine a specific value, and not a range of $DLF$'s in which $DLF_{\mathrm{cr}}$ can be found.

An exact analysis of the course of the curves presented in Figs. 6.16b and 6.17b shows that all the curves are "based" on two straight lines, one descending (for $DLF < 1$) and the other growing (for $DLF > 1$). Each of the curves $r_{\max}$ ($DLF$) has also a non-linear range, which begins after "leaving" the aforementioned straight lines. Comparing the curves and the obtained critical values $DLF_{\mathrm{cr}}$ for the pulse duration $T_{\mathrm{p}} < 0.75\ T$, it can be easily seen that all these curves intersect the line for $r_{\max} = 1$ in the point with the same $DLF$ value. Thus, the criterion proposed by the author has a limit of applicability, because of which it cannot give the critical value of $DLF$ properly for pulse durations less than $0.75\ T$ in this case. Generally, it can be said that the criterion does not provide the correct value of $DLF_{\mathrm{cr}}$ if the curve $r_{\max}$ ($DLF$) intersects the line $r_{\max} = 1$ in its linear part (for example, the curve indicated as '0.001' in Fig. 6.16b or '0.5T' in Fig. 6.17b).

**Table 6.11** Influence of the pulse duration on $DLF_{cr}$

| Pulse duration $T_p$ | Critical value of the dynamic load factor $DLF_{\mathrm{cr}}$ | | | |
|---|---|---|---|---|
| | Budiansky-Hutchinson | Volmir $\xi = 1$ | Author's criterion $r_{max} = 1$ | Inflection point method $P$-$w$ |
| 0.5T | 3.3–3.5 | 3.1 | 2.00 | 4.26 |
| 0.65T | 2.3–2.5 | 2.24 | 2.00 | n/a |
| 0.7T | 2.3–2.5 | 2.06 | 2.00 | n/a |
| 0.75T | 2.1–2.25 | 1.9 | 1.96 | n/a |
| 1T | 1.45–1.5 | 1.46 | 1.45 | 1.52 |
| 1.25T | 1.05–1.2 | 1.29 | 1.24 | n/a |
| 1.5T | 1.05–1.2 | 1.24 | 1.17 | n/a |

Additionally to the orthotropic plates with constant properties, some plates with material properties varying along the width of the plate were also considered. As has been presented in previous author's papers [6, 7] on static buckling and the postbuckling behaviour of structures with widthwise variable material properties, a suitable fibre distribution can lead to an increasing or decreasing buckling load.

Therefore, it was decided to repeat the buckling investigations for plates with widthwise variable material properties but now subjected to the pulse load. An impact of changes in the amplitude $A$ describing the fibre volume fraction $f$ (6.3) along the width of the plate on the course of the curves $\xi$ ($DLF$) and on the critical value of the dynamic load factor $DLF_{cr}$ was investigated. A dynamic response of plates with variable material properties subjected to rectangular pulse with a period of duration equal to a period of fundamental vibrations is shown in Figs. 6.18 and 6.19. The analysed plates are simply supported on all edges (results in Fig. 6.18) and clamped on longitudinal edges (results in Fig. 6.19). The amplitude of initial imperfection $\xi^* = 0.01$ was assumed. The results were obtained with the analytical-numerical method.

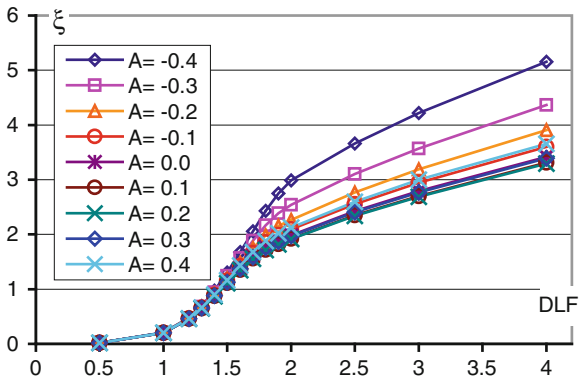


**Fig. 6.18** Curves $\xi$ ($DLF$) for the simply supported plate with a widthwise variable fibre volume fraction

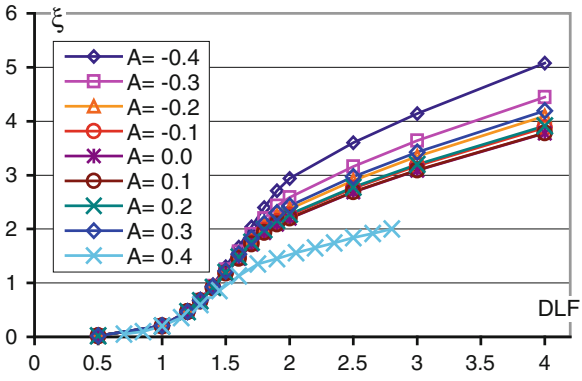


**Fig. 6.19** Curves $\xi$ ($DLF$) for the plate clamped on longitudinal edges with a widthwise variable fibre volume fraction

It can be noticed that the nature of the curves $\xi$ (DLF) for all the boundary conditions taken into consideration is similar, and for small values of the dynamic load factor, i.e., $DLF < 1.5$, the course of the curves defined as the maximum deflection as a function of the dynamic load factor overlap. Only for the case in which the longitudinal plate edges are clamped (Fig. 6.19), the curve for $A = 0.4$ is different from the others. The reason of different behaviour is a different buckling mode ($m = 2$) in this case ($A = 0.4$). To check that all the calculations were correct for that case ($A = 0.4$, clamped longitudinal edges of plate), a comparative analysis was performed—the time courses of the maximum deflection were determined with the analytical-numerical method (MAN) and the finite element method (FEM) and are presented in Fig. 6.20.

The curves shown in Fig. 6.20 were determined for four values of the dynamic load factor $DLF = 1.0$, 2.0, 3.0 and 4.0. The results of both the methods employed are similar for $DLF = 1.0$, and are in accordance to the time when the deflection reached the maximum value for the remaining values of the dynamic load factor. The differences between the results obtained with both the methods became apparent for higher dynamic loads (greater *DLF*), i.e., for $DLF = 3$ or 4, and for the pulse time $t/T_p > 0.7$ (after reaching the first maximum deflection). For those *DLFs,* the buckling mode takes place, and it can be analysed with the finite element method only. Despite these differences, the critical dynamic load factor, determined by displacement criteria (Budiansky-Hutchinson or Volmir) based on the time courses of the maximum plate deflection, obtained with both the methods (MAN and FEM), are almost identical.

On the basis of the Budiansky-Hutchinson criterion, the Volmir criterion and the proposed modified Kleiber-Kotula-Saran criterion (author's criterion), the critical dynamic load factor $DLF_{cr}$ for the composite square plate with its longitudinal edges simply supported or clamped was determined. The results are summarized in Tables 6.12 and 6.13 and they also confirm that the proposed

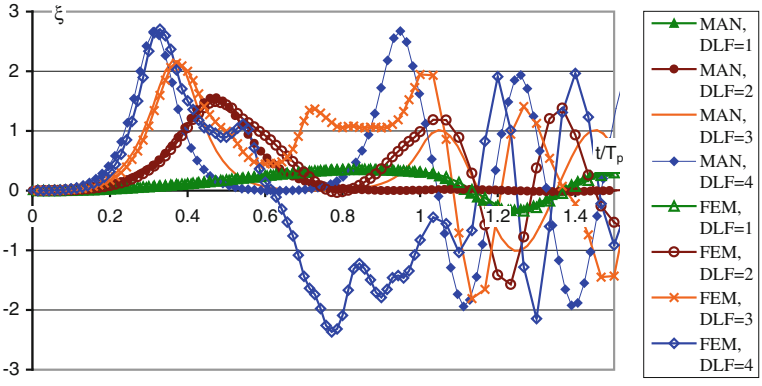


**Fig. 6.20** Time courses of the maximum deflection for the plate clamped on longitudinal edges and subjected to different DLFs—a comparison of calculation methods

**Table 6.12** $DLF_{cr}$ for simply supported plates with a widthwise variable $f$

| Amplitude of sine describing the volume fibre fraction distribution $A$ | Critical value of the dynamic load factor $DLF_{cr}$ | | |
|---|---|---|---|
| | Budiansky-Hutchinson | Volmir $\xi = 1$ | Author's criterion $r_{max} = 1$ |
| −0.4 | 1.6–1.75 | 1.42 | 1.58 |
| −0.3 | 1.45–1.6 | 1.44 | 1.52 |
| −0.2 | 1.6–1.75 | 1.44 | 1.49 |
| −0.1 | 1.45–1.6 | 1.46 | 1.47 |
| 0.0 | 1.3–1.45 | 1.45 | 1.44 |
| 0.1 | 1.3–1.45 | 1.47 | 1.44 |
| 0.2 | 1.45–1.6 | 1.47 | 1.43 |
| 0.3 | 1.3–1.45 | 1.47 | 1.45 |
| 0.4 | 1.45–1.6 | 1.45 | 1.47 |

**Table 6.13** $DLF_{cr}$ for plates clamped on longitudinal edges with a widthwise variable $f$

| Amplitude of sine describing the volume fibre fraction distribution $A$ | Critical value of the dynamic load factor $DLF_{cr}$ | | |
|---|---|---|---|
| | Budiansky-Hutchinson | Volmir $\xi = 1$ | Author's criterion $r_{max} = 1$ |
| −0.4 | 1.6–1.75 | 1.42 | 1.57 |
| −0.3 | 1.45–1.6 | 1.43 | 1.53 |
| −0.2 | 1.45–1.6 | 1.44 | 1.50 |
| −0.1 | 1.6–1.75 | 1.44 | 1.48 |
| 0.0 | 1.45–1.6 | 1.45 | 1.48 |
| 0.1 | 1.45–1.6 | 1.45 | 1.48 |
| 0.2 | 1.45–1.6 | 1.44 | 1.49 |
| 0.3 | 1.45–1.6 | 1.44 | 1.51 |
| 0.4 | 1.3–1.45 | 1.53 | 1.37 |

criterion gives good results for plates with a relatively small amplitude of initial imperfections and subjected to pulse loading with a period of duration equal to a period of natural vibrations. The results presented in Tables 6.12 and 6.13 confirm the previously noticed rule that the critical values of the dynamic load factor $DLF_{cr}$ determined by the proposed criterion are between the critical values obtained from the two well-known criteria (i.e., Budiansky-Hutchinson and Volmir criteria).

Analyzing exactly the results presented in Tables 6.12 and 6.13, one can also notice that the distribution of fibres along the width of the plate has no significant effect on the $DLF_{cr}$ value (the maximum change for the same buckling mode is less than 8 %). If we exclude the case of the clamped plate with $A = 0.4$ due to a different buckling mode, a certain regularity in the value of $DLF_{cr}$ can be observed—the critical value of $DLF$ for the simply supported plate obtained from the Volmir criterion increases with increasing values of $A$ from $A = -0.4$ to $A = 0.3$, and for the plate clamped along its longitudinal edges, the critical value of $DLF_{cr}$ rises for the amplitude $A$ approaching zero ($A = 0$ plate made of a

material of constant properties). The $DLF_{\mathrm{cr}}$ value determined with author's criterion as well as the Budiansky-Hutchinson criterion for simply supported and clamped plates behave conversely—the critical value of *DLF* decreases for the plate with a more uniform distribution of fibres. Strengthening the middle part of the plate ($A = -0.4$) is followed by an increase in a value of the critical dynamic load factor. This is a reverse phenomenon than in the static load case (Fig. 6.4)—the largest amount of the buckling load is for the plate with $A = 0.4$ (reinforced edges).

In the majority of publications dealing with dynamic buckling problems, including the present one, the amplitude of initial imperfections $\xi^* = 0.01$ has been assumed. Such assumption is made only from the numerical point of view. Assuming such a low amplitude of initial imperfections, researchers treat the analysed structures as an almost ideal flat plate. It has been confirmed above by the earlier calculations (Tables 6.3 to 6.5) that the differences between the buckling load for the plate with a low amplitude of initial imperfections $P^*_{\mathrm{cr}}$ and the buckling load for an ideal flat plate $P_{\mathrm{cr}}$ are very small and less than 1 %.

The dynamic load factor *DLF* is defined as a ratio of an amplitude of the pulse load to the critical static buckling load for ideal structures. The calculations presented below were conducted to check how the way *DLF* is estimated influences the critical amplitude of the pulse load leading to the dynamic buckling. The author proposes to introduce a dynamic load factor $DLF^* = P/P^*_{\mathrm{cr}}$—a pulse load amplitude divided by the static buckling load for imperfect structures. As presented in [11], such an approach is very important, especially in the case when the amplitude of initial geometrical imperfections reaches a value equal or higher than $\xi^* = 0.05$.

Some exemplary calculations showing the differences in results according to the way of the *DLF* definition, were performed for the simply supported square plate made of an epoxy-glass composite with the volume fibre fraction $f = 0.5$. Two different periods of pulse duration $T_{\mathrm{p}} = T$ and $T_{\mathrm{p}} = 0.5T$ (where $T$—period of natural fundament flexural vibrations of the plate, for the given material properties and the geometry $T = 0.59$ ms) were assumed.

To show an influence of the assumed amplitude of initial geometrical imperfections and the way of the *DLF* definition on the critical value of the dynamic load factor $DLF_{cr}$, a dynamic response analysis was performed with the analytical-numerical method. In Tables 6.14 and 6.15, the critical dynamic load factors $DLF_{cr}$ (determined in the conventional way) and $DLF^*_{\mathrm{cr}}$ (determined from the $DLF^*(w/h)$ relations, where the amplitude of pulse loading is divided by the buckling load for the plate with initial imperfections), calculated according to the Budiansky-Hutchinson criterion, the Volmir criterion and the inflection point method, are presented.

Analysing the results presented in Tables 6.14 and 6.15, one can say that for low values of the imperfection amplitude (in a range of hundredth parts of the plate thickness), the differences between the critical value of the dynamic load factor known as $DLF_{\mathrm{cr}}$ (a ratio of the critical pulse load amplitude to the static

**Table 6.14** $DLF_{\mathrm{cr}}$ and $DLF^{*}_{cr}$ for different amplitudes of initial imperfections and $T_{\mathrm{p}} = T$

| Assumed criterion: initial imperfection amplitude $\xi^{*}$ | Volmir criterion $\xi_{\mathrm{cr}} = 1$ | Budiansky-Hutchinson criterion | Inflection point method P-w | Volmir criterion $\xi_{\mathrm{cr}} = 1$ | Budiansky-Hutchinson criterion | Inflection point method P-w |
|---|---|---|---|---|---|---|
| | $DLF_{\mathrm{cr}}$ | $DLF_{\mathrm{cr}}$ | $DLF_{\mathrm{cr}}$ | $DLF^{*}_{\mathrm{cr}}$ | $DLF^{*}_{\mathrm{cr}}$ | $DLF^{*}_{\mathrm{cr}}$ |
| 0.01 | 1.49 | 1.4–1.6 | 1.52 | 1.49 | 1.4–1.6 | 1.53 |
| 0.02 | 1.31 | 1.2–1.3 | 1.31 | 1.32 | 1.2–1.3 | 1.32 |
| 0.05 | 1.17 | 0.8–0.9 | 1.14 | 1.21 | 0.9–1.1 | 1.18 |
| 0.1 | 1.07 | 0.8–0.9 | 1.06 | 1.15 | 0.9–1.0 | 1.14 |
| 0.2 | 1.13 | 0.7–0.8 | 0.65 | 1.10 | 0.84–0.96 | 1.10 |
| 0.5 | 0.63 | 0.4–0.5 | 0.49 | 1.08 | 0.7–0.85 | 0.83 |

**Table 6.15** $DLF_{\mathrm{cr}}$ and $DLF^{*}_{cr}$ for different amplitudes of initial imperfections and $T_{\mathrm{p}} = 0.5T$

| Assumed criterion: initial imperfection amplitude $\xi^{*}$ | Volmir criterion $\xi_{\mathrm{cr}} = 1$ | Budiansky-Hutchinson criterion | Inflection point method P-w | Volmir criterion $\xi_{\mathrm{cr}} = 1$ | Budiansky-Hutchinson criterion | Inflection point method P-w |
|---|---|---|---|---|---|---|
| | $DLF_{\mathrm{cr}}$ | $DLF_{\mathrm{cr}}$ | $DLF_{\mathrm{cr}}$ | $DLF^{*}_{\mathrm{cr}}$ | $DLF^{*}_{\mathrm{cr}}$ | $DLF^{*}_{\mathrm{cr}}$ |
| 0.01 | 3.07 | 4.4–4.6 | 4.26 | 3.08 | 4.4–4.6 | 4.27 |
| 0.02 | 2.47 | 3.4–3.6 | 3.57 | 2.49 | 3.4–3.6 | 3.61 |
| 0.05 | 1.89 | 2.0–2.8 | 2.04 | 1.86 | 2.5–2.9 | 2.56 |
| 0.1 | 1.40 | 1.6–1.8 | 1.81 | 1.51 | 1.7–1.9 | 1.95 |
| 0.2 | 1.01 | 1.0–1.2 | 1.17 | 1.21 | 1.2–1.4 | 1.41 |
| 0.5 | 0.62 | 0.4–0.6 | – | 1.01 | 0.7–1.0 | – |

bifurcational load) and the proposed definition of the critical value of the dynamic load factor $DLF^{*}_{cr}$ (a ratio of the critical pulse load amplitude to the static buckling load for the imperfect plate) are less than 1 % and the curves are practically identical (see Figs. 6.21, 6.22 and 6.23). However, for the initial imperfection amplitude $\xi^{*} \geq 0.05$, the differences between $DLF_{\mathrm{cr}}$ and $DLF^{*}_{cr}$ grow with an increasing amplitude of initial geometrical imperfections. The calculations with a new definition of the dynamic load factor $\mathrm{DLF}^{*}$ were carried out once again. The results obtained with the analytical-numerical method for the plate with all types of boundary conditions (Fig. 6.2) subjected to the rectangularly shaped pulse load with the time duration $T_{\mathrm{p}} = T$ or $T_{\mathrm{p}} = 0.5T$ are presented in Tables 6.16 and 6.17.

To make the differences between the results obtained on the assumption of various definitions of the dynamic load factor more visible, the courses of $DLF$ $(\xi)$ and $DLF^{*}$ $(\xi)$ for three values of imperfection amplitudes and two pulse durations ($T_{\mathrm{p}} = 1T$ and $T_{\mathrm{p}} = 0.5T$) are presented in Figs. 6.21, 6.22 and 6.23. In these figures, the static postbuckling curves $P/P_{cr}$ (for the flat plate) and $P/P^{*}_{cr}$ (for the imperfect plate) are also drawn.

It can be noticed that for a relatively small imperfection amplitude $\xi^{*} = 0.01$ (Fig. 6.21), the curves $DLF$ $(\xi)$ and $DLF^{*}$ $(\xi)$ cover each other for the given pulse

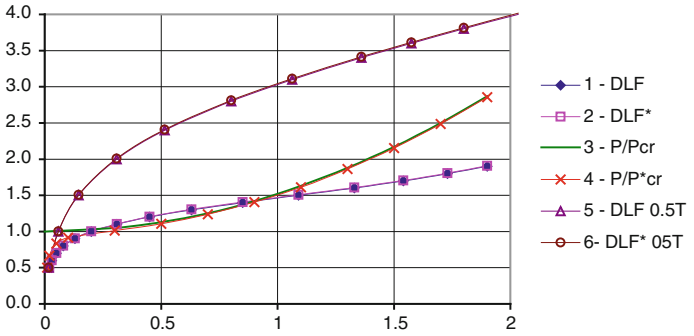


**Fig. 6.21** Static and dynamic responses versus dimensionless deflection for $\xi^* = 0.01$

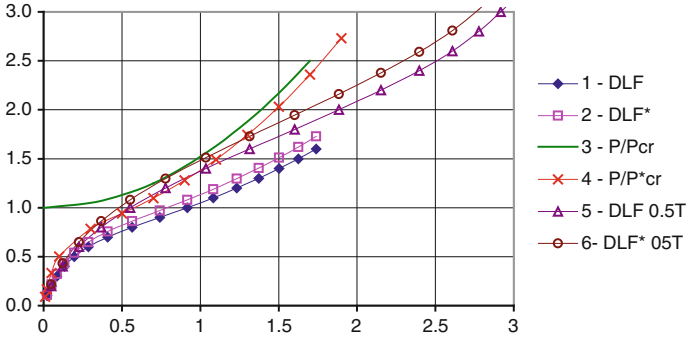


**Fig. 6.22** Static and dynamic responses versus dimensionless deflection for $\xi^* = 0.1$

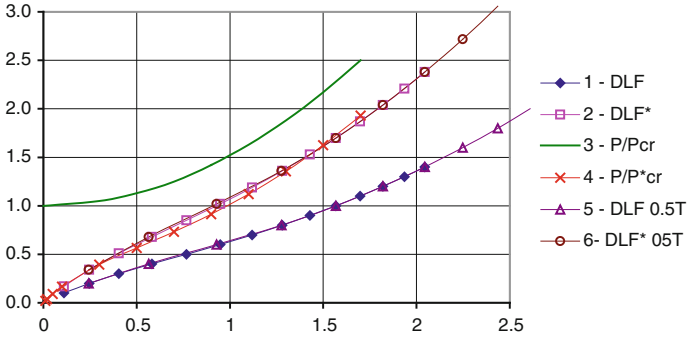


**Fig. 6.23** Static and dynamic responses versus dimensionless deflection for $\xi^* = 0.5$

duration $T_p$. Also the static postbuckling curves overlap (excluding the initial range of deflections). In this case, the character of dynamic responses strongly depends on the assumed pulse duration—for a shorter pulse, the deflections are

**Table 6.16** $DLF^*_{cr}$ determined using different methods/criteria for $T_p = 1T$

| Amplitude of initial imperfections $\xi^*$ | Boundary conditions | Method/criteria | | |
|---|---|---|---|---|
| | | Inflection point method P-w | Volmir criterion $\xi_{cr} = 1/\xi_{cr} = 0.5$ | Budiansky-Hutchinson |
| 0.01 | se | 1.14 | 1.71/1.16 | 1.2–1.4 |
| 0.1 | | 0.38 | 1.39/0.80 | 0.8–1.0 |
| 0.5 | | 0.27 | 0.82/0.39 | 0.2–0.3 |
| 0.01 | ce | 1.10 | 1.78/1.18 | 1.2–1.4 |
| 0.1 | | 0.33 | 1.46/0.82 | 0.8–1.0 |
| 0.5 | | 0.24 | 0.87/0.40 | 0.2–0.3 |
| 0.01 | ss | 1.45 | 1.40/1.06 | 1.4–1.6 |
| 0.1 | | 0.68 | 1.04/0.70 | 0.8–1.0 |
| 0.5 | | 0.43 | 0.63/0.35 | 0.4–0.5 |
| 0.01 | sc | 1.45 | 1.40/1.06 | 1.4–1.6 |
| 0.1 | | 0.67 | 1.04/0.71 | 0.8–1.0 |
| 0.5 | | 0.43 | 0.63/0.34 | 0.4–0.5 |
| 0.01 | cc | 1.52 | 1.36/1.04 | 1.4–1.6 |
| 0.1 | | 0.72 | 0.99/0.69 | 0.8–1.0 |
| 0.5 | | 0.51 | 0.61/0.34 | 0.5–0.6 |

**Table 6.17** $DLF^*_{cr}$ determined using different methods/criteria for $T_p = 0.5T$

| Amplitude of initial imperfections $\xi^*$ | Boundary conditions | Method/criteria | | |
|---|---|---|---|---|
| | | Inflection point method P-w | Volmir criterion $\xi_{cr} = 1/\xi_{cr} = 0.5$ | Budiansky-Hutchinson |
| 0.01 | se | 3.92 | 3.32/2.36 | 3.8–4.2 |
| 0.1 | | 1.10 | 1.52/0.93 | 1.2–1.4 |
| 0.5 | | 0.29 | 0.82/0.39 | 0.3–0.4 |
| 0.01 | ce | 3.84 | 3.34/2.39 | 3.8–4.2 |
| 0.1 | | 0.99 | 1.57/0.94 | 1.2–1.4 |
| 0.5 | | 0.26 | 0.87/0.40 | 0.2–0.3 |
| 0.01 | ss | 4.51 | 3.08/2.12 | 4.6–5.0 |
| 0.1 | | 1.75 | 1.36/0.91 | 1.6–1.8 |
| 0.5 | | 0.50 | 0.64/0.35 | 0.5–0.6 |
| 0.01 | sc | 4.52 | 3.08/2.12 | 4.6–5.0 |
| 0.1 | | 1.76 | 1.36/0.91 | 1.6–1.8 |
| 0.5 | | 0.50 | 0.64/0.35 | 0.5–0.6 |
| 0.01 | cc | 4.56 | 3.01/2.07 | 4.6–5.0 |
| 0.1 | | 1.87 | 1.34/0.90 | 1.8–2.0 |
| 0.5 | | 0.59 | 0.62/0.35 | 0.5–0.6 |

small and the dynamic buckling load is at least three times greater (compare the results in Tables 6.14 and 6.15 or in Tables 6.16 and 6.17).

When the amplitude of imperfections grows up to the value $\xi^* = 0.1$ (Fig. 6.22), the differences between the $DLF$ and $DLF^*$ curves are clearly visible for both pulse durations and the static postbuckling curves $P/P_{cr}$ (for the flat plate) and $P/P_{cr}^*$ differ as well. The character of dynamic responses for the pulse durations $T_\mathrm{p} = 1T$ and $T_\mathrm{p} = 0.5T$ is similar but the dynamic buckling load for a shorter pulse is twice as high as for $T_\mathrm{p} = 1T$.

For small values of the imperfection amplitude (in a range of hundredth parts of the plate thickness), the pulse load duration time strongly affects the dynamic buckling load value and the character of the dynamic response of the plate under consideration.

For a relatively large value of amplitude of initial geometrical imperfections $\xi^*$ (the imperfection amplitude equals half of the plate thickness), the results show (Fig. 6.23) that dynamic responses of the plate do not depend on the pulse load duration—the relations $DLF$ $(\xi)$ for both the assumed periods of the pulse duration (i.e., $T_\mathrm{p} = 1T$ and $T_\mathrm{p} = 0.5T$) overlap and the curves $DLF^*$ $(\xi)$ for both the assumed pulses overlap as well. Moreover, the courses of $DLF^*$ $(\xi)$ are almost identical as the static postbuckling curve $P/P_{cr}^*$. It should be underlined that the differences between the courses of $DLF$ and $DLF^*$ are clearly visible.

One can conclude from the above mentioned observations that for considerably large values of the imperfection amplitude ($\xi^* > 0.1$), an influence of the pulse duration on the courses of $DLF$ $(\xi)$ and $DLF^*$ $(\xi)$ has shown to be negligible. However, the dynamic responses presented as $DLF$ $(\xi)$ and $DLF^*$ $(\xi)$ differ significantly. Additionally, it should be strongly underlined that the proposed relations $DLF^*$ $(\xi)$ calculated for two considered values of pulse load durations are almost identical with the static postbuckling curve $P/P_{cr}^*$, which means that the static and dynamic behaviour of the plate is practically the same for a high amplitude of initial geometrical imperfections. This fact can be only observed if the proposed definition for $DLF^*$ is applied in the calculations.

## References

1. Ari-Gur J, Simonetta SR (1997) Dynamic pulse buckling of rectangular composite plates. Compos B 28B:301–308
2. Jones RM (1975) Mechanics of composite materials. International student edition. McGraw-Hill Kogakusha, Ltd, Tokyo
3. Kelly A (ed) (1989) Concise encyclopedia of composite materials. Pergamon Press, Oxford
4. Kowal-Michalska K (ed) (2007) Statecznosc dynamiczna kompozytowych konstrukcji plytowych. WNT, Warsaw
5. Krolak M (ed) (1990) Stany zakrytyczne i nosnosc graniczna cienkosciennych dzwigarow o scianach plaskich. PWN, Warsaw – Lodz
6. Kubiak T (1998) Nieliniowa analiza statecznosci ortotropowych cienkosciennych pretow o roznych ksztaltach przekrojow poprzecznych, PhD thesis. Technical University of Lodz Press, Lodz

7. Kubiak T (2001) Postbuckling behavior of thin-walled girders with orthotropy varying widthwise. Int J Solids Struct 38(28–29):4839–4856
8. Kubiak T (2005) Dynamic buckling of thin-walled composite plates with varying widthwise material properties. Int J Solids Struct 45:5555–5567
9. Kubiak T (2005) Dynamic buckling of thin composite plates. In: Proceedings IUTAM symposium on multiscale modelling and fracture processes in composite materials, Springer, pp 123–130
10. Kubiak T (2006) Kryterium statecznosci dla konstrukcji cienkosciennych obciazonych impulsowo. In: Proceedings of stability of structure XI-th symposium, Zakopane, Poland
11. Kubiak T, Kowal-Michalska K (2012) A new approach to dynamic buckling load estimation for plate structures. In: Proceedings of Stability of Structures 13-th Symposium, Zakopane, Poland, pp 397–406
12. Petry D, Fahlbusch G (2000) Dynamic buckling of thin isotropic plates subjected to in-plane impact. Thin Wall Struct 38:267–283
13. Simitses GJ (1987) Instability of dynamically loaded structures. Applied Mech Rev 40(10):1403–1408
14. Simitses GJ (1990) Dynamic stability of suddenly loaded structures. Springer Verlag, New York
15. Simitses GJ (1996) Buckling of moderately thick laminated cylindrical shells: a review. Compos B 27B:581–587